Acta Cryst. (1998). D**54**, 707

Low-resolution structural characterization of the arginine repressor/activator from *Bacillus subtilis*: a combined X-ray crystallographic and electron microscopical approach. Erratum

Nicholas M. Glykos,[a] Andreas Holzenburg[b] and Simon E. V. Phillips[a]* at [a]*Department of Biochemistry and Molecular Biology, University of Leeds, Leeds LS2 9JT, England, and* [b]*Department of Biology, University of Leeds, Leeds LS2 9JT, England. E-mail: sevp@bmb.leeds.ac.uk*

(*Received 30 March 1998*)

Abstract

In the paper by Glykos, Holzenburg & Phillips [*Acta Cryst.* (1998). D**54**, 215–225] the name of the second author is given incorrectly. The second author is Holzenberg as shown above.

Acta Cryst. (1998). D**54**, 215–225

Low-Resolution Structural Characterization of the Arginine Repressor/Activator from *Bacillus subtilis*: a Combined X-ray Crystallographic and Electron Microscopical Approach

NICHOLAS M. GLYKOS,[a]† ANDREAS HOLZENURG[b] AND SIMON E. V. PHILLIPS[a]*

[a]*Department of Biochemistry and Molecular Biology, University of Leeds, Leeds LS2 9JT, England, and* [b]*Department of Biology, University of Leeds, Leeds LS2 9JT, England. E-mail: sevp@bmb.leeds.ac.uk*

(*Received 25 April 1997; accepted 7 July 1997*)

Abstract

Attempts to determine the X-ray crystal structure of the intact homohexameric arginine repressor/activator from *B. subtilis* have so far been unsuccessful. The major problem appears to be the lack of an isomorphous heavy-atom derivative with a manageable number of substitution sites. Here it is shown how electron microscopy of thin three-dimensional crystals, the same as those used for the X-ray crystallographic studies, made it possible (i) to obtain experimental support for some conclusions drawn on the basis of X-ray data alone, (ii) to determine the low-resolution distribution of electron density in several different crystallographic projections, and (iii) to obtain a tentative low-resolution model of the whole hexamer.

1. Introduction

In the presence of L-arginine AhrC (the arginine repressor/activator from *B. subtilis*) represses the transcription of the genes encoding the anabolic and activates those encoding the catabolic enzymes of arginine metabolism (Smith *et al.*, 1986, 1989; North *et al.*, 1989).

AhrC is a homohexamer of total molecular mass 105 kDa (Czaplewski *et al.*, 1992). It shows no homology to any of the characterized DNA-binding motifs or DNA-binding proteins with the exception of ArgR, the arginine repressor from *Escherichia coli* (Lim *et al.*, 1987). ArgR does not act as a transcriptional activator, but it has been shown to be a necessary accessory protein for the resolution of the ColE1 plasmid (Stirling *et al.*, 1988). Although the two proteins share only 29% amino-acid sequence identity, and are from such taxonomically distinct prokaryotes, AhrC can complement *E. coli* ArgR$^-$ strains both in the regulation of arginine metabolism and the resolution of the ColE1 plasmid (Stirling *et al.*, 1988; Smith *et al.*, 1989). It is worth noting that the reverse is not true: ArgR cannot complement *B. subtilis* AhrC$^-$ strains in the regulation of arginine metabolism.

Mutational analysis of ArgR (Tian & Maas, 1994; Burke *et al.*, 1994) suggested that the C-terminal region is implicated in arginine binding and oligomerization, whereas the N-terminal region is involved in DNA recognition and binding. The suggested organization of ArgR and AhrC in two functionally and structurally distinct domains has recently been confirmed by the crystal structure determination of the hexameric core fragment of ArgR (Van Duyne *et al.*, 1996).

We have been studying AhrC crystallographically for a number of years (Boys *et al.*, 1990). Three crystal forms have been produced and characterized. An extensive search for useful heavy-atom derivatives resulted in only one possibly useful compound. Numerous attempts to determine the heavy-atom structure of this derivative using the majority of methods in the crystallographic armoury have all failed to give a convincing solution, probably because of the very large number of substitution sites arising from the high non-crystallographic symmetry. Recent attempts to determine the crystal structure of AhrC using the hexameric core fragment of ArgR as a search model in molecular replacement calculations also failed to give a consistent solution.

The presence of high non-crystallographic symmetry offered the possibility of determining the structure of AhrC through a different approach: if a low-resolution model of the crystal structure could be obtained by an independent method, such as electron microscopy, it was hoped that real-space averaging combined with solvent flattening would be powerful enough to refine and extend the phase information to a resolution sufficient for determining (i) the heavy-atom positions of our best derivative, and, (ii) the position and orientation of the ArgR core fragment. Here we present results from our attempt to determine the low-resolution crystal structure of AhrC using a combination of X-ray crystallography and electron microscopy.

2. Materials and methods

2.1. *Protein purification and crystallization*

AhrC was purified as described by Czaplewski *et al.* (1992). We characterized three different crystal forms of AhrC, all grown from low ionic strength solutions.

† Present address: Foundation for Research and Technology-Hellas, Institute of Molecular Biology and Biotechnology, PO Box 1527, 71110 Heraklion, Crete, Greece.

Table 1. *Statistical information for data sets collected from a native and two derivatized orthorhombic AhrC crystals*

Data set	Resolution (Å)	R_{symm} (%)	Completeness (%)	Multiplicity
Native	3.5	7.3	80	1.2
Nb_6Cl_{14}	5.0	3.6	96	1.2
H_2IrCl_6	5.0	3.5	99	1.3

The major form is orthorhombic, space group $C222_1$ with $a = 231.3$, $b = 74.4$, $c = 138.0$ Å and one hexamer in the asymmetric unit. These crystals diffract to ~3 Å resolution on a conventional X-ray source and were obtained using hanging-drop vapour diffusion [protein solution: 50 μ*M* TPCK,† 1.25 m*M* DTT, 1.2 m*M* PMSF, 30 m*M* sodium phosphate buffer pH = 7.5, 150 m*M* ammonium sulfate, 1%(*v*/*v*) 2-propanol, 10 mg ml^{-1} AhrC. Well solution: 50 μ*M* TPCK, 1.25 m*M* DTT, 1.2 m*M* PMSF, 100 m*M* phosphate buffer pH = 4.9, 60 m*M* ammonium sulfate, 1%(*v*/*v*) 2-propanol, 4% PEG 4000. Drops: 4 μl protein plus 4 μl well solution]. This form has been used for most of the crystallographic and electron microscopic experiments.

The second form is monoclinic, space group $P2_1$ with $a = 202.7$, $b = 72.6$, $c = 73.0$ Å, $\beta = 97.8°$ and two hexamers in the asymmetric unit. These crystals diffract to approximately 4 Å resolution on a conventional X-ray source and were again obtained by hanging-drop vapour diffusion [protein solution: 50 μ*M* TPCK, 1.25 *M* DTT, 0.7 m*M* PMSF, 30 m*M* sodium phosphate buffer pH = 7.5, 150 m*M* ammonium sulfate, 1%(*v*/*v*) 2-propanol, 10 mg ml^{-1} AhrC. Mixing solution: 50 μ*M* TPCK, 1.25 m*M* DTT, 0.7 m*M* PMSF, 30 *M* sodium phosphate buffer pH = 7.5, 150 m*M* ammonium sulfate, 1%(*v*/*v*) 2-propanol, 8% PEG 6000. Well solution: 50 μ*M* TPCK, 1.25 m*M* DTT, 0.7 m*M* PMSF, 100 *M* phosphate buffer pH = 5.2, 16 m*M* ammonium sulfate, 1%(*v*/*v*) 2-propanol, 4.4% PEG 6000. Drops: 4 μl protein plus 4 μl mixing solution].

The third form belongs to the trigonal system, but because of its inherent disorder, it has not been possible to characterize it any further.

2.2. *X-ray crystallographic data collection and processing*

More than 80 data sets have been collected from both native and derivatized orthorhombic AhrC crystals. The great majority of these were recorded with an X-100A Xentronics/Siemens, multiwire, position sensitive, two-dimensional area detector. The X-ray source was graphite-monochromated Cu *Kα* radiation from a Rigaku RU200 rotating anode operating at 2.7 kW with a 200 μm focus. Typical statistics for a native and two derivative data sets are shown in Table 1.

The raw data were processed with *XDS* (Kabsch, 1993). Unless otherwise stated, all crystallographic calculations were performed on an DEC Alpha 4000 using the *CCP*4 suite of programs (Collaborative Computational Project, Number 4, 1994).

2.3. *Preparation of heavy-atom derivatives*

Well over 90 compounds have been screened in more than 200 soaking and co-crystallization experiments (Glykos, 1995). From these, only two compounds showed signs of specific binding without damaging the crystals, and only one, namely the niobium cluster Nb_6Cl_{14}, gave a derivative with the characteristics expected from a well substituted and isomorphous protein derivative, that is: (i) small changes in unit-cell dimensions (<0.3%); (ii) mean fractional isomorphous difference from the native crystals significantly above the noise level and decreasing with increasing resolution; (iii) anomalous differences above the noise level, and, (iv) high values of the linear correlation coefficient between isomorphous difference Patterson functions calculated using different data sets or different resolution ranges from the same data set (Jones & Stuart, 1991).

Numerous attempts to determine the heavy-atom structure of this derivative (Glykos, 1995) have all failed to give a convincing solution. Part of the problem lies almost certainly in the large number of substitution sites, but as Argos & Rossmann (1974, 1976) and also Tong & Rossmann (1993) have shown, knowledge of the orientation of the non-crystallographic symmetry axes can reduce the problem to that of determining the heavy-atom sites in the non-crystallographic asymmetric unit. Unfortunately, the variability in the indications obtained from self rotation functions (Rossmann & Blow, 1962) calculated using different resolution ranges or integration radii, made a confident assignment of the orientation of the non-crystallographic symmetry axes impossible.†

2.4. *Electron microscopy: specimen preparation, data collection and image processing*

Orthorhombic AhrC crystals were crushed in a stabilizing solution consisting of 10% MPD and 100 m*M* acetate buffer at pH = 4.9. A droplet of the solution containing the crystal fragments was transferred to a carbon-coated grid and allowed to stand for approximately 1 min. The fragments were negatively stained with a 2%(*w*/*v*) solution of uranyl acetate in water.

Grids were examined in a Philips CM-10 transmission electron microscope operating at 100 kV. Images were recorded at calibrated magnifications (usually 37 500×) on Agfa Scientia 23 D 56 electron-image sheet film, or

† Abbreviations: TPCK, L-1-tosylamido-2-phenylethyl-chloromethyl ketone; PMSF, phenylmethyl sulfonyl fluoride; DTT, dithiothreitol; PEG, polyethylene glycol; MPD, 2-methyl-2,4-pentatediol; CCD, charge-coupled device.

† Supplementary material, pages 1–4.

later, with a TVIPS TEM-1000 on-line image acquisition and analysis system based on a Photometrics AT 200 Peltier-cooled slow-scan 512 × 512 CCD camera controlled by Photometrics PMIS software. Low-dose imaging conditions have not been used. Fig. 1 is an example of a micrograph showing images of several different projections of orthorhombic AhrC crystals.

The best micrographs were identified by optical diffraction using a He/Ne LASER-powered optical diffractometer and digitized using a Joyce–Loebel microdensitometer with a scan step of 25 μm. Further processing of the digitized micrographs or CCD-recorded images was performed with the MRC/*CCP*4 suite of programs (Crowther *et al.*, 1996) as follows: a well preserved area of the image was extracted (program *BOXIM*), its Fourier transform calculated (program *FFT*), and the transform was masked and back-transformed. If the projection could be identified (from the transform or the filtered image), the reciprocal lattice parameters were refined (program *MMLATREF*), and the amplitudes and phases of the observed reflections were extracted (program *MMBOX*). A program was written which determined and applied the phase shifts needed to move the origin of the image to a permissible for the given plane group position and calculated the mean phase difference between (i) symmetry-related reflections, and, (ii) the observed phase angles and those expected from symmetry considerations (applicable to centrosymmetric terms only).

Fig. 1. Electron micrograph of crushed negatively stained AhrC crystals.

In the final step, the phase angles were set to their expected values, they were combined with the corresponding X-ray amplitudes and an electron-density map of the corresponding crystallographic projection was calculated. For such a map to be a valid representation of the electron-density distribution in the native three-dimensional crystals, it is required that: (i) the phases and amplitudes of the structure factors used for the reconstruction are determined by the contrast between protein and solvent of crystallization and not by the internal structure of the macromolecule. For the resolution ranges attainable by negative staining techniques (approximately 18 Å), this requirement is always satisfied. It is worth noting here that the difference in contrast between protein and solvent in the crystals, and between stain and stain-excluding regions in the micrographs affects only the amplitudes of the reflections, and so does not invalidate the process of combining X-ray amplitudes with electron microscopy phases.

(ii) The combined effect of any artifacts possibly introduced during specimen preparation and data acquisition (such as positive staining, changes in unit-cell dimensions, stain migration, *etc.*) cannot reverse the sign of the strong reflections. Although the validity of this statement can only be proven by an independent technique (such as cryoelectron microscopy), we believe that the agreement between the electron microscopical reconstructions and the conclusions drawn from X-ray data alone (discussed below) suggests that this requirement is also satisfied for the resolution limits of the present analysis.

Finally, we note that for the reconstructions presented in the next section we only used data located before the first zero of the contrast transfer function. In this way, and because X-ray amplitudes are available, no corrections for the transfer function are necessary, thus simplifying the procedure of image reconstruction.

3. Results

3.1. *X-ray crystallographic analysis*

Fig. 2 shows the Harker sections $u = 0.0$, $v = 0.0$ and $w = 0.5$ from a 13–6 Å resolution sharpened isomorphous difference Patterson synthesis for the Nb_6Cl_{14} derivative (coefficients $E_{\Delta F}\Delta F$, where $E_{\Delta F}$ is the normalized structure-factor amplitude corresponding to the observed isomorphous difference ΔF). The large peaks marked as *A*, *B* and *C* on these sections form a self-consistent set of Harker vectors corresponding to a site with coordinates $x = 0.130$, $y = 0.090$ and $z = 0.225$ or equivalent by Patterson symmetry.

The first hint that these peaks arise not from a heavy-atom site but from the parallelism between the crystallographic twofold axes and non-crystallographic evenfold axes present in the heavy-atom structure came from the following geometric argument: if a sphere is a reasonable very low-resolution approximation to the shape of an AhrC hexamer, then its expected radius (based on the mean protein density) is 32 Å. Given that the unit-cell dimensions of the orthorhombic form are a = 231.3, b = 74.4 and c = 138.0 Å, it would appear that there should be little overlap of symmetry-related hexamers along the [010] direction. A simple calculation showed that the closest non-overlapping arrangement of circles in the [010] projection places their centres at x = 0.126, z = 0.212 and equivalent by plane group symmetry. The difference from the values obtained from the difference Patterson peaks is only 0.8 and 1.8 Å along x and z, respectively.

These observations taken together suggest that the position of the molecular centre of an AhrC hexamer in the orthorhombic form is at x = 0.13, y = 0.09 and z = 0.23 (note, however, that the choice of enantiomorph is arbitrary). Schematic diagrams of this model of the crystal packing down the major crystallographic axes are shown in Fig. 3. The molecules form layers parallel to the xy planes, with alternating layers being displaced by approximately 13 Å in a direction parallel to y. Large solvent channels (~40 Å in diameter) run parallel to z. It is worth noting here, that there are no outstanding peaks in native Patterson syntheses calculated using data from several different resolution ranges. A possible explanation for their presence in the isomorphous difference Patterson function of the niobium derivative, is that the symmetry of the heavy-atom structure is accidentally higher than that of the AhrC hexamer.

Further evidence supporting this model of crystal packing came from examination of native low-resolution permutation syntheses (Boyes-Watson & Perutz, 1943; Woolfson, 1954). Fig. 4 shows the four unique permutation maps corresponding to the four strongest low-resolution $h0l$ reflections.† Syntheses (*b*), (*c*) and (*d*) show features that are not consistent with the distribution of density expected from protein crystals: there are peaks of high protein density on the twofolds or mirror lines, the solvent areas are unreasonably large and the density is not connected (as we would expect from a projection that is only one molecule thick). Synthesis (*a*) shows a more or less uniform distribution of connected density with a reasonably small solvent area. The position of the highest peak in this map is consistent with the packing model presented above, and as a whole this map is in very good agreement with electron microscopic images of this projection (Fig. 8*a*).

One final – and rather unexpected – piece of evidence supporting this model of the crystal packing came from the observation that protein phases calculated from any

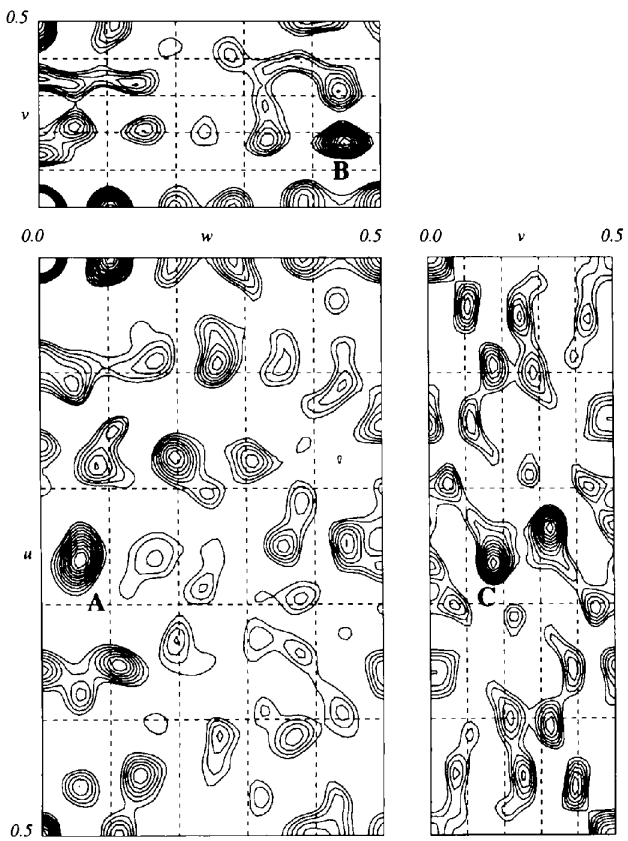

Fig. 2. Harker sections u = 0.0, v = 0.0 and w = 0.5 from a 13–6 Å resolution sharpened isomorphous difference Patterson synthesis for the Nb_6Cl_{14} derivative. Contours every 2% of the origin peak.

† The reflections used for these syntheses are the 201, 202, 002 and 402. The 002 and 402 reflections are structure semi-invariants and all their sign combinations must be examined, but the 201 and 202 reflections belong to two parity groups that can be used to fix the origin and signs can be allotted to them at will, thus leaving only four unique phase combinations of these four terms.

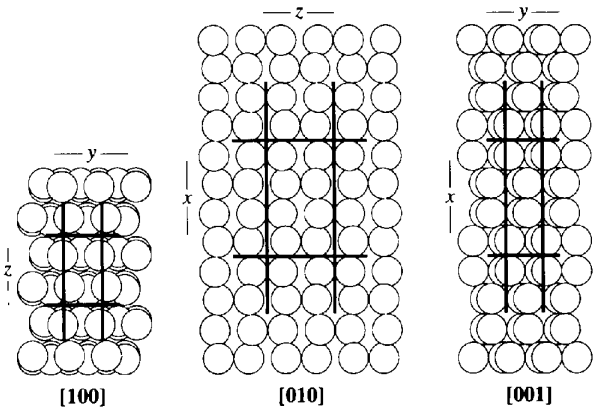

Fig. 3. The crystal packing of the orthorhombic AhrC form. Views of the packing down the [100], [010] and [001] axes are shown. The radius of the spheres (each representing an AhrC hexamer) is 30 Å. In all views 3 × 3 unit cells are shown.

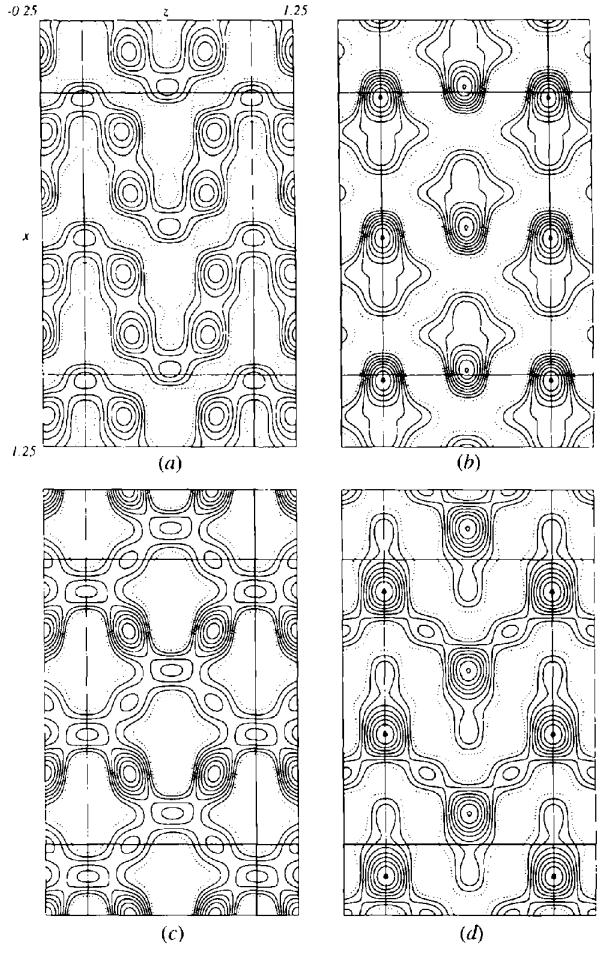

Fig. 4. Permutation syntheses for the [010] projection using the four strongest low-resolution *h*0*l* reflections (see text for details).

heavy-atom structure that can generate the large (pseudo-origin) peaks seen in the difference Patterson synthesis for the niobium derivative, are not random but will lead to electron-density maps with high density at the correct position of the protein molecules.† Fig. 5 shows two [001] projections of native AhrC crystals which were calculated from two unrelated – and incorrect – heavy-atom structures that could nevertheless account for the large pseudo-origin peaks. The presence of well defined solvent channels at the expected (from the crystal packing model) positions is obvious.‡

3.2. *Electron microscopy*

We have identified and characterized images of the [001], [010], [101] and [130] projections of orthorhombic AhrC crystals. From these, the [001] and [010] projections are the best preserved and, thus, the most informative, and will be discussed in some detail.

† See supplementary material, pages 5–7 for results from model calculations.

‡ The first heavy-atom structure consisted of six atoms placed at the corners of a regular octahedron. This octahedron was centered on the molecular centre and oriented in such a way that three orthogonal non-crystallographic twofold axes were parallel with the crystallographic twofold axes. Although this structure could account for several peaks present in the observed difference Patterson synthesis, some of the predicted peaks were displaced with respect to their observed positions by 0.025 along *w*. Upon centrosymmetric refinement all atoms drifted to positions unreastically distant from their starting positions, and the final (refined) heavy-atom structure could not explain the observed isomorphous difference Patterson function. The second heavy-atom structure consisted of a single site at the position of the molecular centre. When this hypothetical heavy-atom site was least-squares refined against all centrosymmetric terms between 15 and 5 Å, it gave statistics of acceptable quality [$R_{\text{Cullis}} = 0.57$, $\text{Corr}(F_o, F_c) = 0.48$], illustrating again the complications arising from the 'special' orientation of the non-crystallographic symmetry elements.

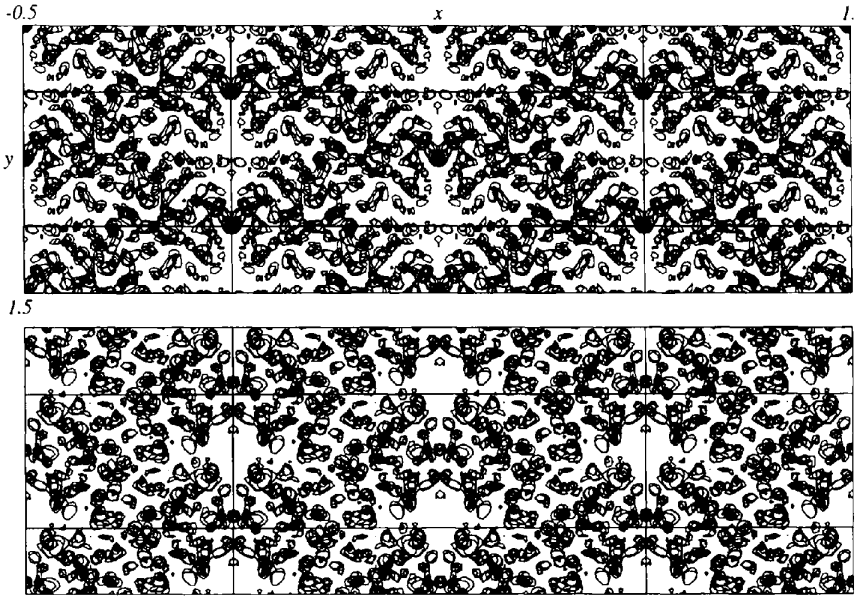

Fig. 5. [001] projections of native AhrC crystals calculated using phases from two unrelated (and incorrect) heavy-atom structures (see text for details).

3.2.1. *The [001] projection*. The great majority of all well preserved areas that have been examined, belong to the [001] projection. This is consistent with the presence of protein layers parallel to the *xy* planes, as already discussed. A typical CCD-recorded image of this projection is shown in Fig. 6(*a*). Most of the [001] images analysed showed reflections out to about 25 Å resolution, although in some cases, periodicities of the order of 18 Å could be detected (Fig. 6*b*). Within the 25 Å sphere, the value of R_{symm} for six pairs of symmetry-related reflections is 20.2%, the mean phase difference from the expected phase angles (0 or π) for 18 observed reflections is 23° and the mean phase difference between symmetry-related reflections is 26.5° (the expected values of these two phase residuals for a random distribution of phase angles are 45 and 90°, respectively). Fig. 7(*a*) shows the 25 Å $F_{X\text{-rays}}\exp(i\varphi_{EM})$ synthesis for this projection and Fig. 7(*b*) is the same map but with its contrast reversed. This should be compared with Fig. 7(*c*) which is a magnified area from the filtered image. Given that map (*c*) has been calculated with amplitudes that have not been corrected for the contrast transfer function, and phases that have not been set to their expected values, the agreement between maps (*b*) and (*c*) is reassuringly good. The density corresponding to two overlapping AhrC hexamers is organized in three interconnected high-density areas (marked as I, II and III in Fig. 7*b*) which surround a central low-density region. The *x* coordinate of the centre of gravity of the three high-density areas is 0.13, in good agreement with the packing model presented above. Because of the overlap, the *y* coordinate cannot be determined accurately, but the diameter of the solvent channels suggests that its value must be close to zero, as expected.

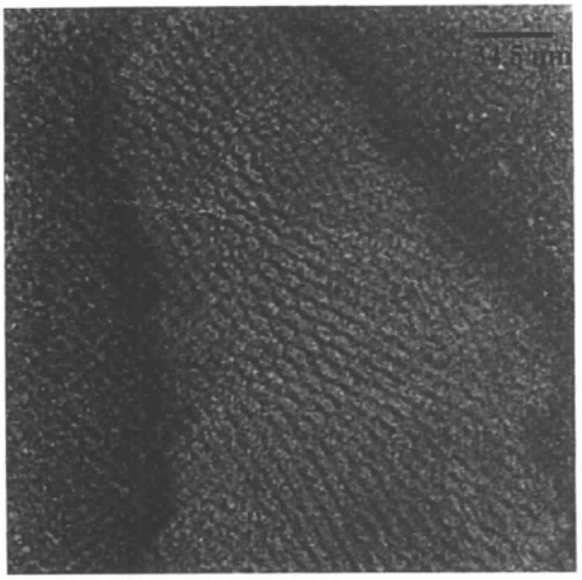

(*a*)

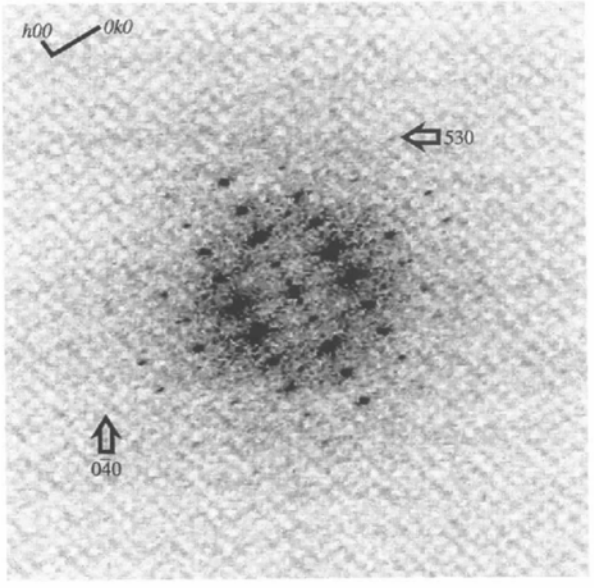

(*b*)

Fig. 6. (*a*) A typical CCD-recorded image of the [001] projection. (*b*) Modulus of the Fourier transform of a well preserved image of the [001] projection. The positions of two weak but observed reflections corresponding to spacings of 21.5 Å (530) and 18.3 Å (040) are indicated.

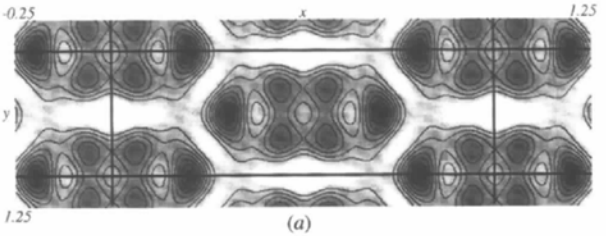

(*a*)

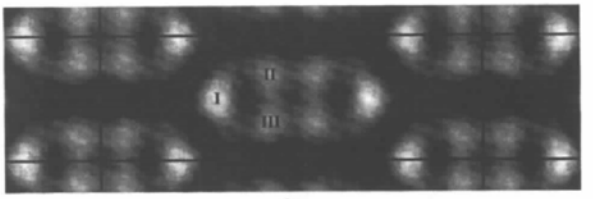

(*b*)

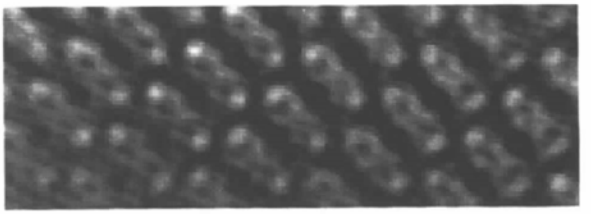

(*c*)

Fig. 7. (*a*) and (*b*) The $F_{X\text{-rays}}\exp(i\varphi_{EM})$ reconstruction of the [001] projection at 25 Å resolution. (*c*) Magnified area from the filtered image.

3.2.2. *The [010] projection*. A magnified area from the original micrograph is shown in Fig. 8(*a*), and 8(*b*) is the modulus of the Fourier transform of a larger area from the same image. Within the 25 Å sphere the R_{symm} for 13 pairs of symmetry-related reflections is 14%, the mean phase difference from the expected phase angles (for 31 reflections) is 21.5° and the mean phase difference between symmetry-related reflections is 35.7°. Fig. 9(*a*) is the 25 Å $F_{X\text{-rays}}\exp(i\varphi_{EM})$ synthesis, and Fig. 9(*b*) is the same map but with its contrast reversed. The reconstruction is in good agreement not only with the original micrograph, but also with the permutation map shown in Fig. 4(*a*) thus confirming again the proposed crystal packing model.

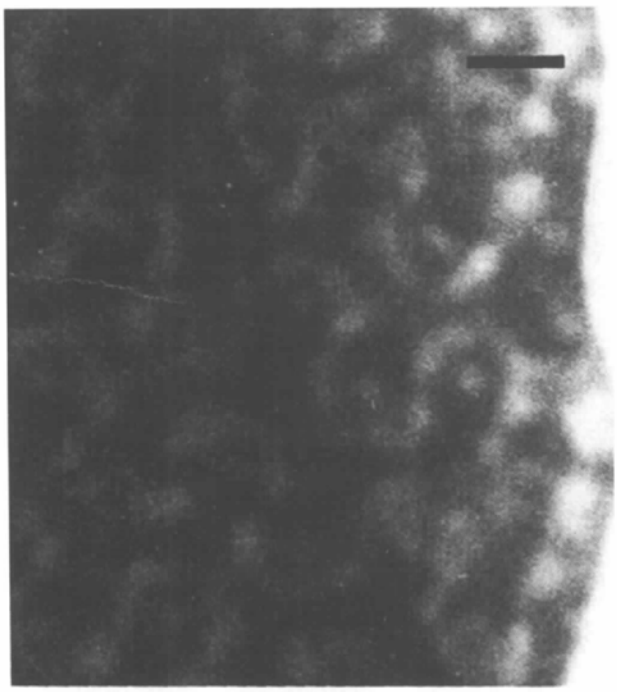

(*a*)

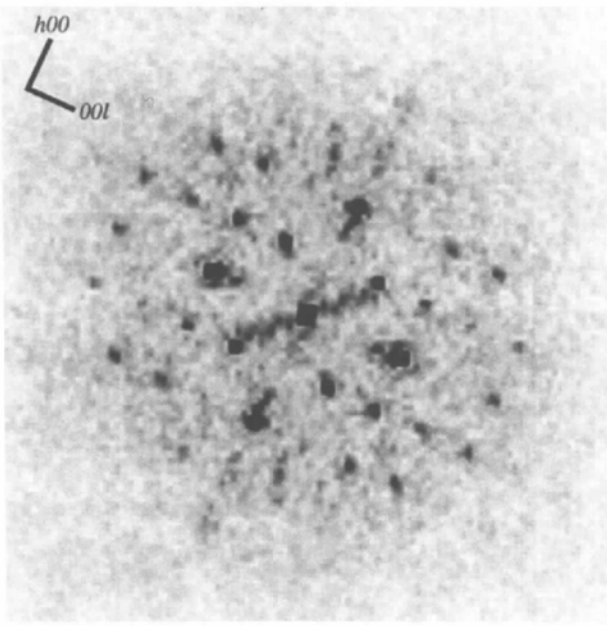

(*b*)

Fig. 8. (*a*) Magnified area from an image of the [010] projection, scale bar = 70 Å. (*b*) Modulus of the Fourier transform of a larger area from the same image.

The density corresponding to a single AhrC hexamer is organized in three high-density areas, marked as I, II and III in Fig. 9(*b*) and a low-density extension, marked as IV. The density for domains I, II and IV is continuous, but the connectivity of area III is not obvious. Although the projection along [010] is only one molecule thick, it is difficult to interpret this electron-density map in terms of a projection of a D_3 hexamer (as expected on the basis of the known structure of the ArgR hexameric core fragment).

3.3. *The calculation of a 30 Å electron-density map*

In the case of the orthorhombic form of AhrC, there are 34 unique reflections within the 30 Å resolution sphere. 91% of these can be measured from five projections (14 reflections from the [010], five from the [001], three from the [130], three from the [100] and six reflections from the [110] projection). Unfortunately – and probably because of the organization of molecules in layers parallel to the *xy* planes – it has not been possible to identify images of the [100] and [110] projections. Attempts to fix the crystals with glutaraldehyde, embed them in a polymer and cut sections perpendicular to the required axes in a ultramicrotome (Labaw & Davies, 1972; Langer *et al.*, 1975) have also failed because of the sensitivity of the AhrC crystals to cross linking: fixing them for 2 h in a solution containing 10% MPD, 100 m*M* acetate buffer at pH = 4.9 and 0.5%(*v*/*v*) glutaraldehyde resulted in a complete loss of the diffraction pattern as judged by precession photography.

Of the 34 unique reflections (to 30 Å resolution), 22 are centrosymmetric of known sign† and 12 are non-centrosymmetric of unknown phase. It was decided to calculate phases for all non-centrosymmetric terms from a model of the electron density consisting of spheres of constant density at all crystallographically equivalent positions of the molecular centre. These would be combined with the experimentally determined signs and a 30 Å three-dimensional electron-density map could be calculated.

The amount of error introduced into the final three-dimensional map from this procedure depends on how

† The signs of the three 0*kl* reflections were determined from examination of very low resolution permutation syntheses as described for the [010] projection.

good model a sphere of constant density is for the given structure. Results from model calculations, shown in Fig. 10, suggest that the map calculated from the mixed phase set can be a reasonable approximation to the true electron density: column (*a*) in this Fig. 10, shows a series of sections through the low-resolution density of a hypothetical model D_3 hexamer placed in the unit-cell and space group of the orthorhombic AhrC form. Column (*b*) shows sections through the model of spheres of constant density used for calculating phases for the non-centrosymmetric terms. Finally, column (*c*) is the electron-density map calculated from the mixed phase set. The agreement between the true and reconstructed density provides convincing evidence that an electron-density map calculated with 35% of the phases coming from a model sphere of constant density can still be a very good approximation to the true density. When these model calculations were repeated with a hypothetical structure for which a sphere of constant density was a bad approximation† the final map was a crude, but not unacceptable approximation to the true density.

Figs. 11(*a*), 11(*b*) and 11(*c*) show three approximately orthogonal views of the three-dimensional model constructed from the 30 Å electron-density map of one AhrC hexamer. The density is organized in six domains (marked I to III and I′ to III′): domains I, II and III are well connected and the same is true for domains I′, II′ and III′. Both trimers are irregular in shape and their relative orientation deviates significantly from that expected from a regular D_3 hexamer. This is shown more clearly in Fig. 11(*d*) which is a view of the model down the approximate threefold axis. Several attempts to refine the phases (at constant resolution) through real-space averaging (Bricogne, 1974, 1976) showed no sign of convergence.

† Supplementary material, pages 8–9.

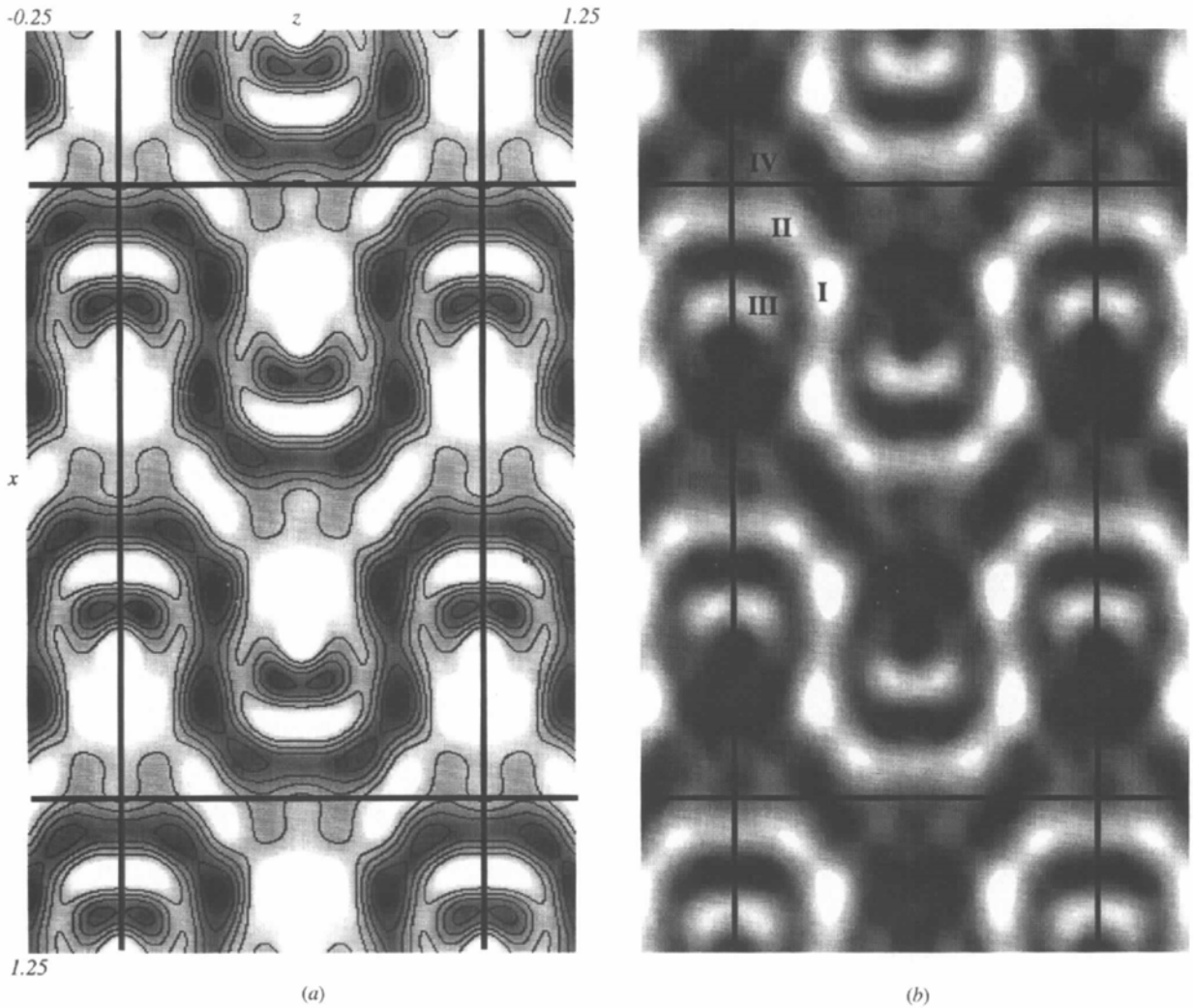

(*a*) (*b*)

Fig. 9. (*a*) and (*b*) The $F_{\text{X-rays}}\exp(i\varphi_{\text{EM}})$ reconstruction of the [010] projection at 25 Å resolution.

4. Discussion and concluding remarks

The analysis of the orthorhombic form of AhrC has almost reached the point of knowing about this form as much as it is possible to know without determining its structure: the X-ray analysis allowed the determination of the crystal packing and showed that in favorable cases examination of the crystallographic symmetry, unit-cell dimensions and of the intensity of very low resolution reflections can give valuable information not only about the crystal packing but also the electron-density distribution. Electron microscopy of negatively stained crystal fragments confirmed the crystal packing model and made possible the experimental determination of the distribution of electron density in several different crystallographic projections. The reassuringly good agreement between the X-ray analysis and the electron microscopical reconstructions agrees well with previous studies (Jack *et al.*, 1975), emphasizes the complementarity of the two methods and suggests that electron microscopy can offer valuable help in those cases where the X-ray analysis alone cannot make progress towards a complete structure determination.

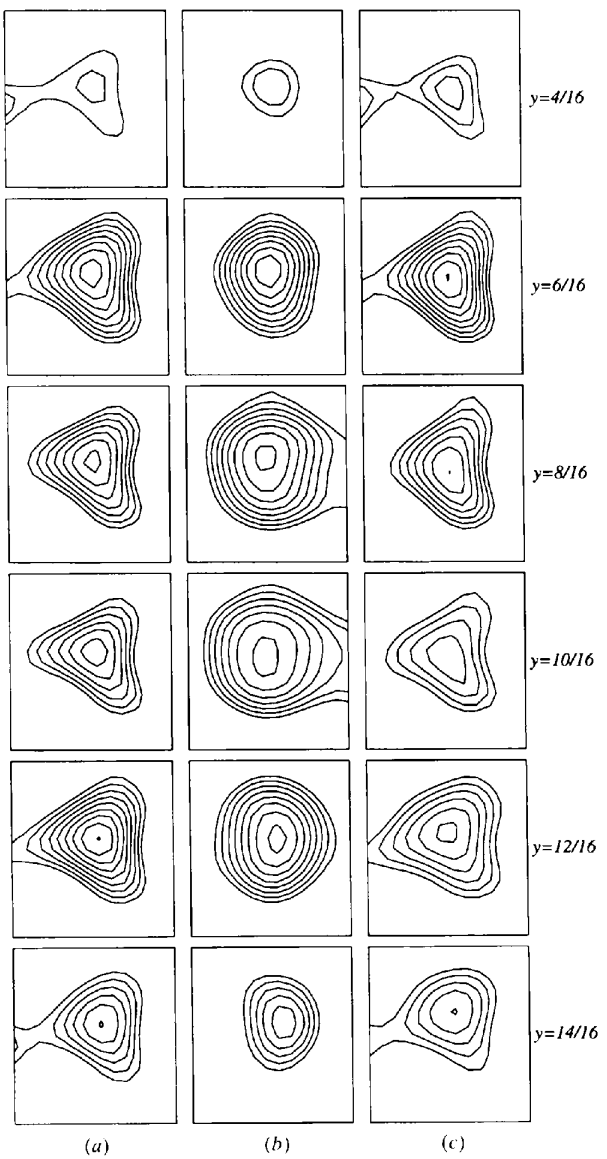

Fig. 10. Sections through (*a*) the density of a hypothetical model D_3 hexamer at 30 Å resolution, (*b*) of a sphere of constant density used for calculating phases for the noncentrosymmetric terms, (*c*) the map calculated with the mixed phase set (see text for details).

The 30 Å three-dimensional reconstruction of AhrC, being based in part on phases calculated from a model, must be treated with caution. The major problem with this reconstruction is the absence of the expected symmetry elements: The known structure of the hexameric core fragment of ArgR has symmetry D_3. Given that AhrC and ArgR share 34% identity in their C-terminal domains, it would be expected that the hexameric core fragment of AhrC should have the same symmetry. Although it is not impossible that the mode of association of the AhrC protomers is indeed different from the one seen in the ArgR structure (noting also that the latter lacks the DNA-binding domains), the amount and quality of the data used for the reconstruction cannot support such a statement.

It is obvious that the long-awaited high-resolution crystal structure of AhrC would not only provide valuable biological insight, but would also answer a series of crystallographic questions concerning the quality of the three-dimensional reconstruction presented above, the symmetry of the AhrC hexamer, and why it could not be identified from the self-rotation functions, the heavy-atom structure of the niobium derivative, and why almost all known methods of structure determination have failed with it.

In an attempt to circumvent AhrC's extreme sensitivity to mercurial reagents, we have expressed and purified site-directed mutants of the protein where each of the two cysteine residues has been replaced in turn by serine (SEVP and Mark R. Parsons, data not shown). Crystallization trials with these mutant forms are currently in progress.

We should like to thank Dr Greg van Duyne and Professor Paul Sigler for making the atomic coordinates of their ArgR model available to us before publication, Drs Coleen Miller, Isobel Parsons and Andrew Walsh for their help with the purification of AhrC, Mr Paul McPhie for expert technical assistance with the electron microscopes and Dr Mark Parsons for useful discussions. We thank the University of Leeds, and the Leeds Centre for Molecular Recognition for support, and the BBSRC for support and a studentship (to NMG). SEVP is an International Research Scholar of the Howard Hughes Medical Institute.

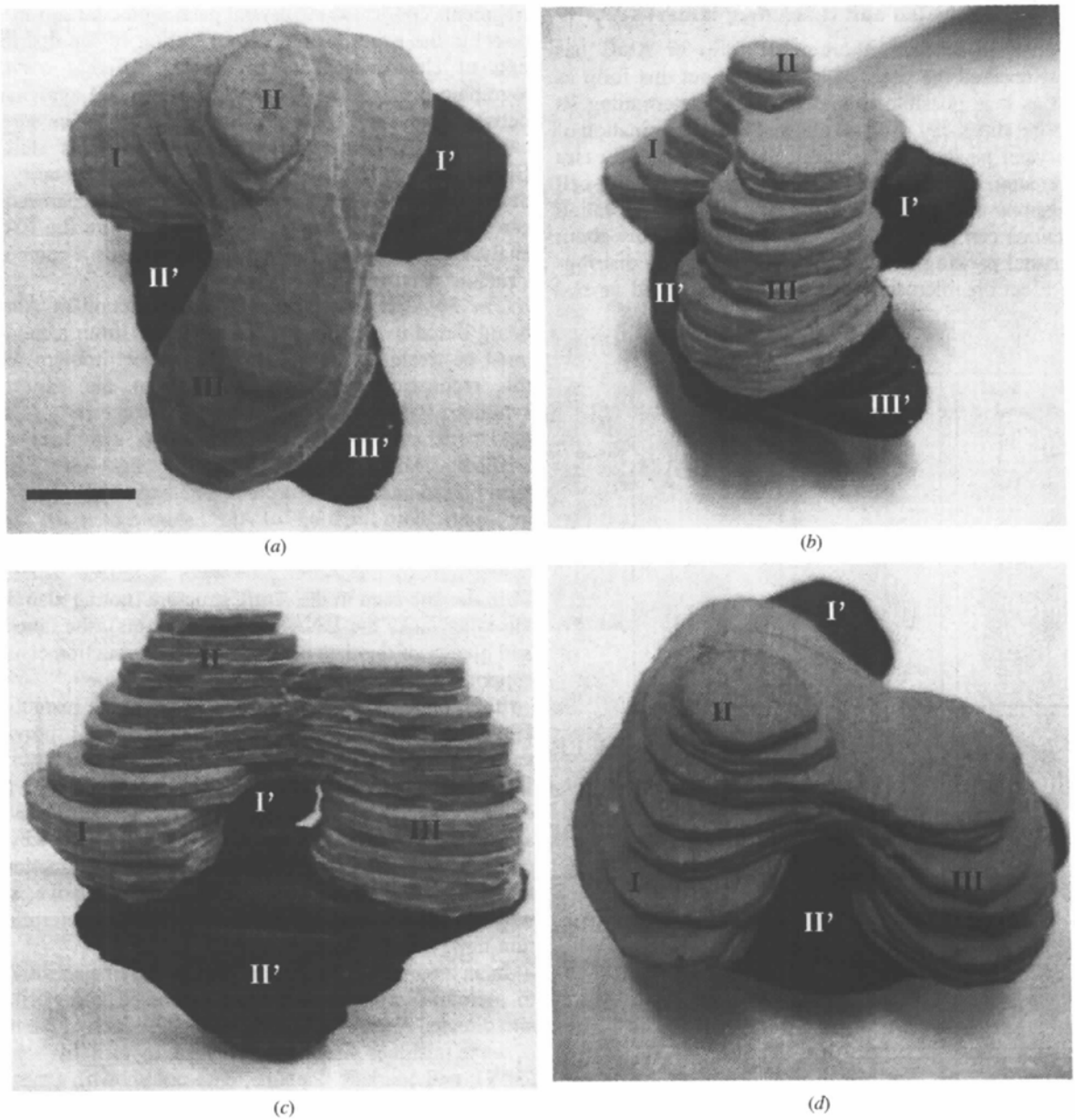

Fig. 11. (*a*), (*b*) and (*c*) three approximately orthogonal views of the three-dimensional model of AhrC constructed from a 30 Å resolution electron-density map. (*d*) View of the same model along the morphological threefold axis. Scale bar = 20 Å.

References

Argos, P. & Rossmann, M. G. (1974). *Acta Cryst.* A**30**, 672–677.

Argos, P. & Rossmann, M. G. (1976). *Acta Cryst.* B**32**, 2975–2979.

Boyes-Watson, J. & Perutz, M. F. (1943). *Nature (London)*, **151**, 714–716.

Boys, C. W. G., Czaplewski, L. G., Phillips, S. E. V., Baumberg, S. & Stockley, P. G. (1990). *J. Mol. Biol.* **213**, 227–228.

Bricogne, G. (1974). *Acta Cryst.* A**30**, 395–405.

Bricogne, G. (1976). *Acta Cryst.* A**32**, 832–847.

Burke, M., Merican, A. F. & Sherratt, D. J. (1994). *Mol. Microbiol.* **13**, 609–618.

Collaborative Computational Project, Number 4 (1994). *Acta Cryst.* D**50**, 760–763.

Crowther, R. A., Henderson, R. & Smith, J. M. (1996). *J. Struct. Biol.* **116**, 9–16.

Czaplewski, L. G., North, A. K., Smith, M. C. M., Baumberg, S. & Stockley, P. G. (1992). *Mol. Microbiol.* **6**, 267–275.

Glykos, N. M. (1995). PhD thesis, University of Leeds, England.

Jack, A., Harrison, S. C. & Crowther, R. A. (1975). *J. Mol. Biol.* **97**, 163–172.

Jones, Y. & Stuart, D. (1991). *Proceedings of the CCP4 Study Weekend 25–26 January, 1991*, pp. 39–48, edited by W. Wolf, P. R. Evans & A. G. W. Leslie. Warrington: Daresbury Laboratory.
Kabsch, W. (1993). *J. Appl. Cryst.* **26**, 795–800.
Labaw, L. W. & Davies, D. R. (1972). *J. Ultrastruct. Res.* **40**, 349–365.
Langer, R., Poppe, C., Schramm, H. J. & Hoppe, W. (1975). *J. Mol. Biol.* **93**, 159–165.
Lim, D., Oppenheim, J. D., Eckhardt, T. & Maas, W. K. (1987). *Proc. Natl Acad. Sci. USA*, **84**, 6697–6701.
North, A. K., Smith, M. C. M. & Baumberg, S. (1989). *Gene*, **80**, 29–38.
Rossmann, M. G. & Blow, D. M. (1962). *Acta Cryst.* **15**, 24–31.
Smith, M. C. M., Czaplewski, L., North, A. K., Baumberg, S. & Stockley, P. G. (1989). *Mol. Microbiol.* **3**, 23–28.
Smith, M. C. M., Mountain, A. & Baumberg, S. (1986). *Mol. Gen. Genet.* **205**, 176–182.
Stirling, C. J., Szatmari, G., Stewart, G., Smith, M. C. M. & Sherratt, D. J. (1988). *EMBO J.* **7**, 4389–4395.
Tian, G. L. & Maas, W. K. (1994). *Mol. Microbiol.* **13**, 599–608.
Tong, L. & Rossmann, M. G. (1993). *J. Appl. Cryst.* **26**, 15–21.
Van Duyne, G. D., Ghosh, G., Maas, W. K. & Sigler, P. B. (1996). *J. Mol. Biol.* **256**, 377–391.
Woolfson, M. M. (1954). *Acta Cryst.* **7**, 65–67.